This article has been accepted for publication in a future issue of this journal, but has not been fully edited. Content may change prior to final publication. Citation information: DOI 10.1109/TETC.2022.3147376, IEEE Transactions on Emerging Topics in Computing

Solar Particle Event and Single Event Upset Prediction from SRAM-based Monitor and Supervised Machine Learning

J. Chen, T. Lange, M. Andjelkovic, A. Simevski, L. Li and M. Krstic

Abstract—The intensity of cosmic radiation may differ over five orders of magnitude within a few hours or days during the Solar Particle Events (SPEs), thus increasing for several orders of magnitude the probability of Single Event Upsets (SEUs) in space-borne electronic systems. Therefore, it is vital to enable the early detection of the SEU rate changes in order to ensure timely activation of dynamic radiation hardening measures. In this paper, an embedded approach for the prediction of SPEs and SRAM SEU rate is presented. The proposed solution combines the real-time SRAM-based SEU monitor, the offline-trained machine learning model and online learning algorithm for the prediction. With respect to the state-of-the-art, our solution brings the following benefits: (1) Use of existing on-chip data storage SRAM as a particle detector, thus minimizing the hardware and power overhead, (2) Prediction of SRAM SEU rate one hour in advance, with the fine-grained hourly tracking of SEU variations during SPEs as well as under normal conditions, (3) Online optimization of the prediction model for enhancing the prediction accuracy during run-time, (4) Negligible cost of hardware accelerator design for the implementation of selected machine learning model and online learning algorithm. The proposed design is intended for a highly dependable and self-adaptive multiprocessing system employed in space applications, allowing to trigger the radiation mitigation mechanisms before the onset of high radiation levels.

Index Terms— solar particle event, single event upset, machine learning, online learning, hardware accelerator, reliability, self-adaptive multiprocessing system

1 Introduction

As CMOS technology scales into the deep nanometer range, the design of integrated circuits (ICs) for space missions becomes more and more challenging. The radiation-induced Single Event Upsets (SEUs) represent one of the main reliability concerns for space-borne ICs. An SEU is a transient bit flip in storage elements such as flip-flops, latches and SRAM cells. This effect may occur when energetic particles (e.g., heavy-ions, alpha particles, neutrons, protons) pass through the sensitive regions within the memory elements. As a result of SEUs, the temporary data corruption and system malfunction could occur. Therefore, the efficient detection and cost-effective mitigation of SEUs in electronic systems for space applications are crucial.

One of the main causes of SEUs in space is the Solar Particle Event (SPE) phenomenon [1]. During an SPE, a large number of energetic particles are emitted into space and this event can last from several hours up to several days. These energetic particles can induce SEUs either by direct ionization or by indirect ionization [2]. Since the particle flux directly determines the SEU rate of an electronic system, based on the data obtained from past space missions [3][4], the SEU rate may increase hundreds to thousands of times during the SPE peak periods. Thus, it is important to track the variation in particle flux in real-time, and consequently activate the suitable mitigation techniques to protect the sensitive elements in the on-board electronic systems. An example is the adaptive multiprocessing system, which can dynamically adapt the rad-hard modes (e.g., core-level triple module redundancy) or low-protection modes (e.g., high performance and low power consumption) as the radiation conditions change [5].

For the detection of SPEs, various commercial or custom-designed particle detectors are use [6]. The particle detectors allow for measuring the particle flux or Linear Energy Transfer (LET) based on the induced soft errors. The most common particle detectors used in space missions are diode- [7] and SRAM-based detectors [8][9][10]. In addition, alternative solutions such as bulk built-in current detectors [11], acoustic wave detectors [12], and 3D NAND flash detectors [13] can be also used. Due to the low implementation cost, SRAM-based detectors have been widely used in space missions. However, the main limitation of existing SRAM detectors is that they are mainly implemented as stand-alone devices. For the self-adaptive systems, however, it is important to measure accurately the radiation exposure that directly affects the target system. Thus, the on-chip radiation detection is imperative.

In order to achieve efficient SEU mitigation and maintain the functionality of the system, it is necessary to enable the real-time flux variations prediction, i.e., to predict the upcoming SPEs. In such a way, radiation protection techniques can be deployed before the burst of particles during SPEs. In order to facilitate the SPE prediction based on real-time SEU detection, various machine learning algorithms can be applied to predict SEU variations. Many works have

- *J.Chen, M. Andjelkovic, A. Simevski, L. Lu are with the IHP – Leibniz-Institut für innovative Mikroelektronik, Frankfurt Oder, Germany. E-mail: {chen, andjelkovic, simevski, lu}@ihp-microelectronics.com.*
- *T. Lange is with the iROC, Grenoble, France and the Politecnico de Torino, Torino, Italy. E-mail: lange@ihp-microelectronics.com.*
- *M. Krstic is with the IHP – Leibniz-Institut für innovative Mikroelektronik, Frankfurt Oder, Germany and the University of Potsdam, Potsdam, Germany. E-mail: krstic@ihp-microelectronics.com.*

This article has been accepted for publication in a future issue of this journal, but has not been fully edited. Content may change prior to final publication. Citation information: DOI 10.1109/TETC.2022.3147376, IEEE Transactions on Emerging Topics in Computing

reported the use of various machine learning algorithms to forecast the onset and duration of SPE, as well as for the characterization and optimization in the rad-hard system design [14][15][16][17][18][19]. However, to the best of our knowledge, there is no much of publicly available work on the use of machine learning algorithms for the prediction of SPEs and SEUs from in-flight detected SEU data, in order to facilitate the self-adaptive mechanisms in space-borne electronic systems.

The aim of this paper is to utilize an embedded on-chip SRAM-based SEU monitor, the supervised machine learning model as well as historical solar events flux data to forecast the in-flight SRAM SEU rate, and thus, the occurrence of the SPEs. The ability to predict accurately the increase in the radiation levels during SPEs minimizes the risk that the target system would be exposed to adverse conditions without being sufficiently protected.

The rest of the paper is structured as follows. Section 2 briefly discusses the state-of-the-art and our contributions. Section 3 provides an overview of the proposed system. The historical solar events analysis procedure is detailed in Section 4. The training and evaluation for supervised machine learning and online learning algorithm are presented in Section 5. Section 6 introduces the architecture of a dedicated hardware accelerator. The analysis of results is detailed in Section 7. Section 8 evaluates the application of the proposed design in the self-adaptive dependable multiprocessing system. This paper is concluded in Section 9.

2 State-of-the-Art and Paper Contributions

2.1 Space Radiation

The space radiation particles can be separated into two categories: particles captured by the planetary magnetosphere in the radiation belt and radiation particles from deep-space [1]. The planetary magnetic fields, such as the Van Allen belt around the Earth, can trap the charged particles, for example, protons, electrons and heavy ions. The radiation field from deep-space consists of Galactic Cosmic Rays (GCRs) and SPEs, which are mainly composed of heavy-ions and protons. GCR comes from outside the solar system and maybe originating from explosive events, e.g., the supernova explosion. The SPEs occur due to the eruptive phenomena in the solar corona, such as the solar flares and Coronal Mass Ejection (CME).

When an SPE occurs, it can become the dominant contributor to the space radiation environment. As a result, the intensity of energetic protons, ions, and electrons in the interplanetary space can be rapidly increased. According to the definition from the National Oceanic and Atmospheric Administration (NOAA) Space Environment Center [20], the start of one SPE is the at least three consecutive five minute intervals flux data points $\geq 10\ cm^{-2}s^{-1}sr^{-1}$ of proton with energy $\geq 10\ MeV$. In addition, the end of the solar event is defined as the last time the flux $\geq 10\ cm^{-2}s^{-1}sr^{-1}$. SPEs may last from several hours to several days, and could reach the peak flux within tens of minutes to several hours, and then slowly decay in several hours to several days. Moreover, the SPE peak flux could be two to five orders of magnitude higher than the background conditions. Thus, the SPEs could be strong enough to cause hazards in space applications. For example, the measured SEU rate of a 4k*32 bit 0.25 μm CMOS SRAM module in a geostationary satellite during a few SPEs is illustrated in Table I [21]. The approximate value of the background upset rate is obtained by linear fitting to the monthly average data.

TABLE I
Upset Rates ($upsets.bit^{-1}.day^{-1}$) In A Geostationary Satellite During Large SPEs

Data	Background	Worst five Minutes	Worst Day	Worst Weeks
April 15,2001	3.7×10^{-8}	3.8×10^{-5}	6.1×10^{-7}	1.3×10^{-7}
Nov. 5,2001	3.8×10^{-8}	2.5×10^{-5}	7.4×10^{-7}	2.1×10^{-7}
Oct. 28,2003	4.4×10^{-8}	2.5×10^{-5}	6.1×10^{-7}	2.1×10^{-7}
Jan. 20,2005	8.1×10^{-8}	2.4×10^{-5}	6.5×10^{-7}	2.3×10^{-7}

2.2 Prediction of Space Radiation Effects

In the recent past, different machine learning algorithms have been employed for the forecasting of space weather in the space missions for various purposes, such as planning spacecraft and satellite routes/manoeuvres, protecting astronauts, etc. E. Camporeale et al. reviewed the current achievements, forecasting opportunities and future role of machine learning in space weather [14]. In [15], H. M. Bain et al. applied the machine learning classification techniques on the existing Space Weather Prediction Center (SWPC) statistical proton prediction model. The result showed that the machine learning model could make a much faster decision than the previous numerical models. A NASA-invest space intelligence system was proposed by A.J. Engell [16], which had the capability for the forecasting of solar-driven events and provided the high fidelity as well as pre-to-post eruptive transitional forecasts.

However, the SPEs could not be reliably predicted since the current quantitative prediction methods (e.g., [22]) require the continuous data, such as particle flux data, flare location, radio burst data, etc. R. Glein et al. [23] used the BRAMs embedded in an FPGA as the particle detector and counted the corresponding SEUs to determine the radiation condition. In addition, by calculating the mean time between failures based on four measured points, the SPE onset can be timely detected [24], but this approach cannot provide fine-grained monitoring of SPE variations.

The machine learning methods have been also used in the rad-hard system design, such as the optimization of the Soft Error Rate (SER) characterization. F. Rocha de Rosa et al. [17] applied the supervised and unsupervised machine learning techniques on the multicore system, for the purposed of soft error analysis. In [18], T. Lange et al. used the machine learning algorithms to optimize the fault-injection simulation campaigns as well as evaluate the system functional failure rate. S. Hirokawa et al. [19] exploited the machine learning method to facilitate soft error discrimination method, and verified the importance of the multiple sensitive volume method.

This article has been accepted for publication in a future issue of this journal, but has not been fully edited. Content may change prior to final publication. Citation information: DOI 10.1109/TETC.2022.3147376, IEEE Transactions on Emerging Topics in Computing

2.3 Our Contributions

In contrast to the state-of-the-art solutions for the SPE and SEU prediction discussed in Section 2.2, we predict the upcoming SPE by achieving the fine-grained SEU prediction, thus, forecasting the solar condition and the system reliability variations. The presented paper extends our previous work [25][26] by implementing the online adjustment of the prediction function parameters, and enhancing the functionality of the hardware accelerator, which are to the best of our knowledge not feasible with any of the reported design. Additionally, we have analyzed the application of the proposed design in a fault-tolerance multiprocessing system, in order to enable the self-adaptive optimal mitigation techniques selection.

Our solution supports a supervised machine learning model to provide a fine-grained prediction of the SRAM SEU rates at least 1 hour in advance. Moreover, an online learning method, which can further improve the prediction accuracy of machine learning in real-time, is introduced. The use of online adjustment allows adapting the system to completely unexpected situations which could not be predicted based on the offline training.

A low-cost hardware accelerator is customized to execute the proposed machine learning prediction model and online learning algorithm. The cost and area/power overheads of the proposed hardware accelerator are negligible compared to the host SRAM. Besides that, the application of the proposed design in the self-adaptive fault-tolerance multiprocessing system is analyzed, allowing to trigger the optimal SEU mitigation methods under variable radiation conditions.

3 System Overview

Our approach for the SPEs and SEUs prediction flow is illustrated in Fig. 1. The basic principle is the prediction of the in-flight SEU count rate of an on-board SRAM-based SEU monitor. Therefore, the upcoming SPEs can be detected from the rise of the predicted SEU rate. The main reason for using the prediction together with the SEU measurement, rather than just measuring the SEU rate, is to minimize the possible adverse impact of radiation on the system operation. Namely, if only the SEU measurement is employed, it may be too late to react once the SEU is detected, because the monitor needs a certain time period to collect and process the information.

The proposed method consists of two phases:

Offline phase – application of historical space flux data (from previous space missions) to establish a suitable SEU prediction machine learning model.

Online phase – measurement of the real-time in-flight SRAM SEU count rate, and the prediction of upcoming SEU changes.

There are two main blocks in the offline phase: solar condition analysis and supervised machine learning. In the solar condition analysis block, the in-flight hourly Soft Error Rate (SEU rate) of the target SRAM during several historical solar events is determined, which is discussed in Section 4. The collected hourly SEU rates are processed for training in the supervised machine learning block. Based on the off-line training, a suitable SEU prediction model can be obtained, which is described in Section 5.

The online phase contains two main blocks: real-time SEU detection and hardware accelerator. The real-time SEU detection is performed continuously during the mission. Most existing SRAM-based monitors [8][9][10] have been implemented as stand-alone particle detectors. However, for the self-adaptive systems for space applications it is important that the particle monitor is embedded into the target system in order to detect the radiation conditions to which the target system is exposed during the mission. An embedded low-cost SRAM-based SEU monitor is intended to be used in the online phase for the real-time SEU measurement [27]. It is essential to mention that the existing SRAM resources are utilized for SEU measurement, which minimized the area and power overhead.

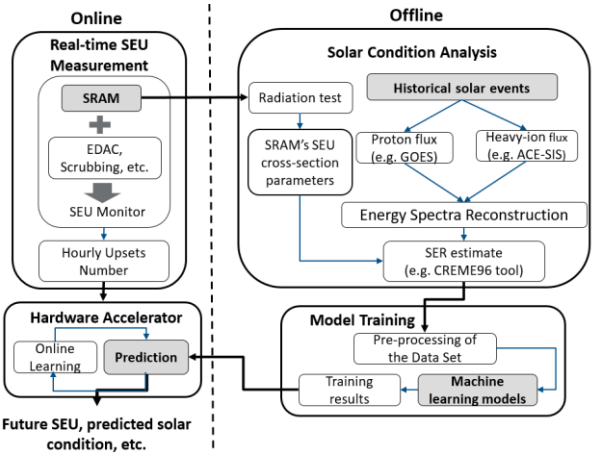

Fig. 1. Block diagram of the proposed prediction method.

Using the scrubbing approach, Error Detection and Correction (EDAC) code, and the over-counting detection register file with a dedicated detection flow [27], the proposed monitor can ensure accurate counting of all upsets that occur in the target SRAM, and distinguish the error type in each memory word. Appropriate EDAC codes can be selected and implemented with the dedicated detection flow for the detection or correction of SEUs, Multiple-Cell Upsets (MCUs) and permanent faults on memory words, such as SEC-DED (Single Error Detection-Double Error Correction), SEC-DAEC-TAEC (Double Adjacent Error Correcting-Triple Adjacent Error Correction), 3-bit burst ECC [27], etc. Therefore, bit errors and the corresponding error type in each memory word can be accurately detected. Moreover, in order to provide further protection against multiple-bit errors in each memory word, we aim to apply the well-known interleaving technique. This technique can distribute the memory cells from the same word into different columns, so that they are physically distant from each other and the probability that a single particle hits multiple bits of the same word is drastically reduced. Thus, MCUs in different memory words can be corrected or detected by the EDAC code, and the MCUs in the same memory word can also be mitigated by using the interleaved SRAM technology. In these ways, the proposed

This article has been accepted for publication in a future issue of this journal, but has not been fully edited. Content may change prior to final publication. Citation information: DOI 10.1109/TETC.2022.3147376, IEEE Transactions on Emerging Topics in Computing

monitor can provide the accurate in-flight fault counting capability during run-time, which is essential for the following prediction.

The number of detected SEUs per hour is stored and processed by the hardware accelerator. The hardware accelerator implements the off-line trained machine learning model and the online learning algorithm. The online learning algorithm is used in order to enhance the accuracy of prediction, since the off-line training model may not take into account all realistic scenarios, as discussed in Section 5.4. Therefore, the predicted SEU data can be collected and the improvement of the prediction accuracy can also be achieved during the runtime, which is detailed in Section 6. Moreover, Triple-Module Redundant (TMR) flip-flops [28] are used in components of the online phase to enhance the robustness against radiation particles.

The functionality of SRAM may also be affected by Single Event Functional Interrupts (SEFIs) and Single Event Latchup (SEL) or micro-SEL. It is thus imperative to apply appropriate design measures to mitigate these effects. Since the SEFIs are caused by particle strikes in control logic, one such event may result in hundreds or thousands of upsets. To mitigate these effects, the control logic should be protected with radiation-hardening-by-design techniques. We aim to investigate various selective protection schemes at multiple abstraction levels, such as the combination of gate-level TMR and error detection and correction. We have already conducted extensive research in relation to SEL protection, and have proposed an SEL protection switch (SPS) based on inverter as an SEL sensor [29]. The SPS detects excessive supply current flow, as a key manifestation of SEL, and restarts the power to restore the normal operation. It has been tested on a real chip with around 20 000 on-chip SPS cells. Irradiation tests have shown that a chip with SPS is immune to SEL at a maximum tested LET of 67 MeVcm^{2}mg^{-1} [29].

4 Solar Condition Analysis

The procedure to obtain the in-flight SEU rate from historical solar events flux data is introduced in this section. This procedure provides the training data for the machine learning block. The general steps of this process are:

1) Historical space flux data collection;
2) SPE energy spectra reconstruction;
3) SRAM SEU rate estimation.

4.1 Flux Data Collection

In this study, in order to ensure that the selected solar events are comprehensive and representative, according to the statistics from NOAA [20], all 36 SPEs which affected the earth environment during the solar cycle 24 (2008-2019) are selected as analyzing target. There are several satellites and instruments that have continuously measured the space ions flux during the selected events. For the target of this study, satellites located close to the Earth in the heliosphere and outside the Earth's magnetic influence are preferred, where the additional radiation impact from geomagnetically trapped ions and the shield protection from the Earth's magnetic field can be neglected. As a result, the Geostationary Operational Environmental Satellite-Space Environment Monitor (GOES-SEM) [30] and Advanced Composition Explorer-Solar Isotope Spectrometer (ACE-SIS) [31] public databases have been used for proton and heavy-ion flux data source, respectively. The GOES-SEM database has continuously provided high-quality proton data since 1974. The ACE-SIS database continues to provide [He, C, N, O, Ne, Na, Ma, Al, Si, S, Ar, Ca, Fe and Ni] flux data since 1997.

4.2 SPE Energy Spectra Reconstruction

The differential flux for each ion needs to be processed in order to obtain the energy spectrum, which is required for the SEU rate estimation. In this study, the target is to reconstruct the hourly average energy spectrum for the ions and protons, which is a total of 5107 hours for the selected events. The flux data obtained from online databases cannot directly be used for the SEU rate estimation due to: (i) limited types of detected heavy ions, (ii) insufficient energy range, and (c) ion flux data gaps. The common approach to solve the above problems is to generate the mission flux data from composition ratios with existing flux information [32].

The CREME 96 [33] suite, which is one of the most widely used suites for evaluating the in-orbit SEU rate, was used to assist the analysis and verification in this study. The CREME96 SPE models (peak five minutes (P5M), worst week (WW), and worst day (WD)) are based on the corresponding average flux data of the October 1989 event, which is one of the largest events in past decades.

$$\sigma(x) = \begin{cases} \sigma_{sat}\,(1 - e^{-(\frac{x-x_0}{w})^s}), & \text{if } x > x_0 \\ 0, & \text{if } x \le x_0 \end{cases} \quad (1)$$

The target SRAM in this study is the COTS SRAM from Cypress which is designed in 65 nm bulk CMOS technology. In [34], a series of heavy ion and proton radiation tests have been carried out on the target SRAM, and the experimental data has been fitted to the Weibull function, defined by Eq. (1). The Weibull function is characterized by four parameters: the on-set parameter (x_0), the saturation cross-section (σ_{sat}), the width parameter (W), and the dimensionless exponent (S). In Eq. (1), since the Weibull curve is used for fitting heavy-ion and proton cross-section data, the x represents either the LET for heavy-ions or the energy for protons, and x_0 is the LET or energy threshold.

There are in total four types of the SRAM cross-section values obtained from [34]: bit or event cross-section with static or dynamic operating mode, respectively. The event cross-section is calculated by counting the number of events as opposed to the number of bit flips. Whereas bit cross-sections allow a representation of the SEE sensitivity of the memory from a usage perspective looking at the output of how many bits are flipped. Moreover, in the CREME96 HUP model, heavy-ion cross-section must be specified in bits for the direct ionization-induced SEU rate evaluation. Besides that, there is a difference in the SRAM cross-section depending on the operating mode (static or dynamic). Since the target SEU monitor does not degrade

This article has been accepted for publication in a future issue of this journal, but has not been fully edited. Content may change prior to final publication. Citation information: DOI 10.1109/TETC.2022.3147376, IEEE Transactions on Emerging Topics in Computing

the basic function of the target SRAM, the SRAM could work in read/write (dynamic) or idle (static) modes. After evaluating the static and dynamic SRAM cross-sections on the CREME96 SPE models, it was observed that higher SEU rate occurs in static mode. Therefore, as a proof of concept, the SRAM radiation test result of bit cross-section in static mode is used in this study. The static Weibull fitting parameters for heavy-ion and proton bit cross-section of the target SRAM are shown in Table II. For heavy-ion cross-section parameters, the σ_{sat} is in cm²/bit, the x_0 means the LETth in MeVcm2mg-1, and W is also in MeVcm²mg⁻¹. For proton cross-section parameters, the σ_{sat} is in cm²/bit, the x_0 means the E_{th} in MeV, and W is also in MeV.

TABLE II
WEIBULL FITTING PARAMETERS OF THE TARGET SRAM HEAVY-ION AND PROTON STATIC BIT CROSS-SECTION

	δ_{sat}	x_0	W	S
Heavy-ion	7.90×10^{-8}	1.04	23.57	1.43
Proton	1.97×10^{-13}	3.00	5.02	0.95

Since the ACE-SIS database only provides 14 types of heavy-ion flux data, it is important to analyze the effect of limited types of heavy-ions for this study. Table III describes the target SRAM SEU rate estimated for all ions from He (2) to U (92) and the ACE-SIS detected ions by using the CREME96 SPE models, respectively. The results show that in all three SPE models, the error caused by the incompletely detected ion type is less than 1%. Therefore, by only using the ACE-SIS ions for the heavy-ion-induced upsets analysis is accepted. However, the energy range of the ACE-SIS is from 5 to 150 MeV, which is quite low and insufficient for the following SEU rate estimations. In order to reconstruct a suitable energy spectrum for ACE-SIS ions with a proper energy range, i.e., from 1 MeV to 1 GeV, the first order power-law fit [35] is used to extrapolate to a higher energy range. Moreover, the simple moving average process was applied to evaluate the hourly fluxes date when the source data is invalid at some moments.

TABLE III
SRAM SEU RATE ($upsets.bit^{-1}.day^{-1}$) SENSITIVITY TO IONS WITH DIFFERENT CREME96 SPE MODELS

Ions	Worst Weeks	Worst Day	Worst Five Minutes
He(2)-U(92)	6.97357×10^{-5}	3.20759×10^{-4}	1.19209×10^{-3}
ACE-SIS	6.97202×10^{-5}	3.20716×10^{-4}	1.19194×10^{-3}

The proton data from the GOES database has been available in good quality and sufficient energy range (over 700 MeV) for the energy spectra reconstruction. In this study, the first-order exponential in rigidity approach is applied for the proton data. The mathematical fitting expression is:

$$\varphi(>E) = N_0 e^{-R/R_0} \quad (2)$$

where the $\varphi(>E)$ is the integral energy fluence in proton/cm², N_0 is a normalization constant, R is the proton rigidity (proton momentum) in MV (million volts), and R_0 is the characteristic rigidity in MV. The proton rigidity R is related to the proton energy (MeV) by:

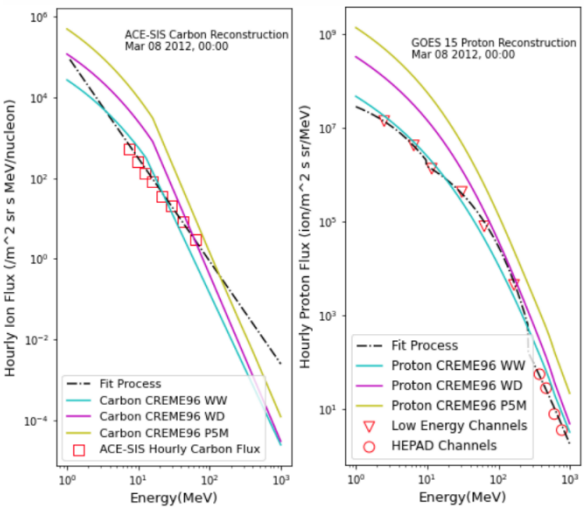

Fig. 2. March 08, 2012, 00:00, ACE-SIS Carbon and GOES-15 proton reconstructed hourly energy spectra with respect to the CREME96 SPE models, respectively. Dashed lines correspond to the corresponding extrapolation method flux fitting results. Squares correspond to the ACE-SIS hourly carbon flux. Triangles correspond to the hourly proton in the GOES low energy detector. Circles correspond to the hourly proton in the GOES HEPAD detector.

$$R(MV) = \sqrt{E^2 + 2m_0 E} \quad (3)$$

where the E is the proton energy in MeV and $m_0$is the rest mass of proton (938 MeV). Since the above approach fit performs not so well when the energy is very low, the power-law fit method is used when E is less than 10 MeV. In addition, the proton energy spectrum needs to be estimated in the same range as the heavy-ion. Thus, the high energy range proton data (HEPAD energy channel, greater than 375 MeV for GOES 15) was extrapolated with the power-law fit. Fig. 2 shows the ACE-SIS Carbon ion and GOES 15 proton one-hour average flux data and the corresponding fit-extrapolation obtained with respect to the CREME96 SPE models, respectively. The reconstructed hourly spectrum for March 08, 2012, 00:00, which is before the peak of one solar event.

4.3 SEU Rate Estimation

By applying the reconstructed energy spectra and the target SRAM cross-section parameters in the CREME96 suite, the hourly SEU rate for the selected events can be obtained. The device shielding is critical for space applications, thus, the first step is to obtain effective energy spectra after the shielding. Since this study was not aimed at specific space projects, a 100 mils of aluminum shielding was assumed, which is the conventional equivalent shielding thickness for spacecraft [34].

Since the heavy-ion-induced SEUs depends on the energy deposition, but not the number of hits like proton-induced SEUs, the Sensitive Volume (SV) geometry is needed for the SEU rate estimation. The CREME96 suite

This article has been accepted for publication in a future issue of this journal, but has not been fully edited. Content may change prior to final publication. Citation information: DOI 10.1109/TETC.2022.3147376, IEEE Transactions on Emerging Topics in Computing

uses the RPP model (Rectangular Parallelepiped Parallelogram) [36] for direct ionization induced upset events calculation, in which the bit SV is assumed to have this shape. Choosing the RPP thickness that conforms to the device cross-section direction dependence is not trivial [21].

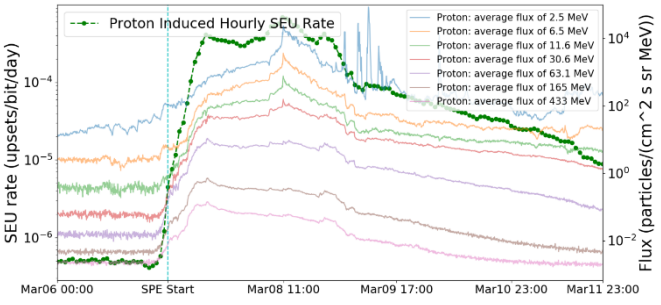

Fig. 3. March 6-11, 2012 SRAM hourly SEU rate estimated from GOES proton database. The particle flux for all of the lower to higher energy channels are shown, and all channels data are with good quality.

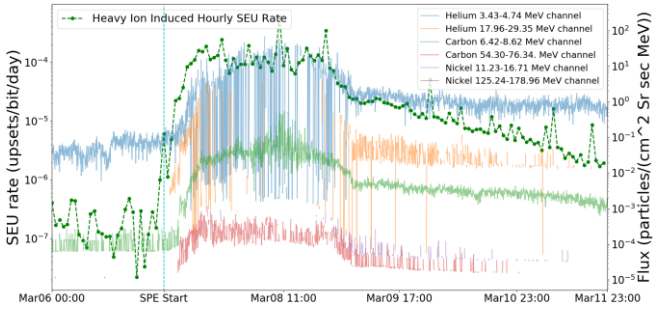

Fig. 4. March 6-11, 2012, SRAM hourly SEU rate estimated from ACE-SIS heavy-ion database. The particle ion flux of He, C and Ni for the lower and higher energy channels are shown, and the data are with poor quality.

For the sake of simplicity, the RPP value recommended by CREME96 was selected, in which lateral dimensions x and y are determined as the square root of the limiting cross-section for each bit, and the device depth z is 0.5 um. The saturation cross-section can be determined from the Weibull fitting as illustrated in Table. II. Applying the above parameters in the CREME96 suit, the heavy-ion-induced and proton-induced hourly SEU rate can be obtained, respectively. Figs. 3 and 4 present the obtained proton-induced and heavy-ion-induced hourly SEU rate with respect to the corresponding ion flux from March 6 to 11, 2012, respectively. The final hourly SEU rates for target SRAM during the selected events are the sum of calculated proton and heavy-ion induced SEU rate.

5 SEU Prediction with Machine Learning

This section elaborates how machine learning techniques can be applied for early detection of the SEU rate changes. The SEU prediction is intended to operate in conjunction with real-time in-flight SEU measurement and the approach aims to predict fine-grained SEU rate in advance by using the upset rates of the n_h last hours provided from the SEU monitor. Therefore, several machine learning regression models have been trained and evaluated to select the optimal model, which yields the best prediction accuracy. In addition, an online learning method is evaluated in order to increase the prediction accuracy during the online phase.

The regression models were selected based on a low-resource demand. The model training was conducted offline in a supervised manner by applying the estimated SEU data from past events. In this way, an already trained model can be used online to perform the prediction, which generally needs fewer computation resources.

To perform the training of the machine learning models, first, the in-flight hourly SEU rate data acquired from historical solar events are processed and transformed in order to be representative to actual upsets obtained from the SEU monitor (as described in Section 3). After, the machine learning regression model is trained with the transformed data acquired from historical solar events. Then, the accuracy of the trained model to predict the hourly upset rate is evaluated. These steps are described in detail in the following sections. Additionally, an algorithm is analyzed to perform online learning after the model is deployed.

5.1 Pre-processing of the Data Set

The in-flight hourly SEU rate data acquired from historical solar events form the test and training data set for the machine learning models. The hourly SEU rate values are obtained by processing the hourly flux database, as explained in Section 4. The processed hourly flux data together with the cross-section of the target SRAM are used to calculate the hourly SEU rate by using the CREME96 suite. In this way the SEU/bit/day is obtained. Since in the actual system, the data from the SEU monitor will be an integer ranging from 0 to the size of the SRAM, the calculated SEU/bit/day are multiplied by the target SRAM size. In this study, the SRAM size of 2G bit is selected, which can provide enough detected SEU resolution during any solar events. Further, to get the hourly upset rate, the SEU/bit/day values are divided by 24h. Thus, the SEU rate per hour is obtained as it would be measured from the SEU monitor in the actual system.

Most machine learning models do not perform well when the input data has a wide numerical range. Therefore, a min-max scaling was applied to the data before the training, which scales the input data to a range from 0 to 1. This is archived by dividing the hourly SEU rate, obtained from the previous step, by the next power of two of the highest expected number of upsets. In this way, no actual division needs to be implemented in hardware since it is just a different representation of the input data as a fixed point integer.

5.2 Model Training

The transformed and pre-processed data is used to train and evaluate different machine learning regression models in a supervised manner. The data set was split, where 60% of the data was used to train the model and the remaining 40% of the data was used to evaluate the model. In this

This article has been accepted for publication in a future issue of this journal, but has not been fully edited. Content may change prior to final publication. Citation information: DOI 10.1109/TETC.2022.3147376, IEEE Transactions on Emerging Topics in Computing

study, five well-known regression models have been analyzed: (1) Linear Regression, (2) Decision Tree Regression, (3) k-Nearest Neighbors Regression, (4) Multi-Layer Perceptron (MLP) Neural Network and (5) Recurrent Neural Network (RNN) with Long Short-Term Memory (LSTM). The Python´s Scikit-Learn [37] and Kearas [38] frameworks were used to implement the above models.

Usually, machine learning models have internal parameters or use internal states to adjust their algorithm and to perform an accurate prediction. These parameters are determined and optimized based on the training data during the training process. In addition to the internal parameters, most of the machine learning models also have external parameters, which are called hyperparameters. These hyperparameters are often used to tune the training algorithm, which determines the internal parameters. Thus, contrary to the internal parameters, hypermeters cannot be determined by the training algorithm itself. They need to be specified manually by the user before the training process. In order to find the optimal set of hyperparameters of a model, a hyperparameter optimization has to be performed. Therefore, the model is trained and evaluated several times with different sets of hyperparameters.

In this paper, the hyperparameters are determined by performing a random search coupled with grid search [39]. In this approach, the models are firstly evaluated with randomly generated hyperparameter values. Then, a more detailed grid search is performed within the region of the best hyperparameter values obtained by the random search.

Besides the hyperparameters, the performance of the model also depends on the amount of past hourly SEU rate values are used for the prediction. The length n_h describes how many hours of past SEU rate values are used. Similar to the hyperparameter optimization, the optimal length for n_h needs to be determined, thus, models were also evaluated for different history length of the hourly SEU data.

5.3 Model Evaluation

To evaluate the prediction performance of a model, in this study, the root-mean-square error (RMSE) and the coefficient of determination (R^2) metrics are used. The RMSE describes the square root of the quadratic error of the expected values. In comparison to the mean absolute error, the root-mean-square error gives a higher weight to larger errors which are then penalized more. The R^2 score is a combined evaluation metric which takes the RMSE and the variation (dispersion) of the model into account. Thus, the R^2 score provides a measure of how well future samples are likely to be predicted by the model. These metrics were calculated by comparing the test data set with the predicted test data set of the trained model.

In order to obtain a more stable measurement, a cross-validation strategy with a cross-validation fold of 10 was used. In this strategy, the data set is split into 10 different train and test data sets which are used to independently train and evaluate the models. Then, the calculated metrics for each independently trained and evaluated model are averaged over the different measurements.

The performance of the models was evaluated for different length n_h of the past hourly SEU data, considering the hourly intervals between 3 h and 24 h. For each considered n_h, the above described hyperparameter optimization was performed, and the model performance was measured according to the specified metrics. Fig. 5 and 6 respectively show the R^2 scores and RMSE for each regression model on different history data length. It can be seen that both the RNN with LSTM and the linear regression model have the highest accuracy, and the performance of the RNN is slightly better. The best performances are obtained with a past hourly SEU data n_h of 14 for the RNN and 17 for the linear regression model.

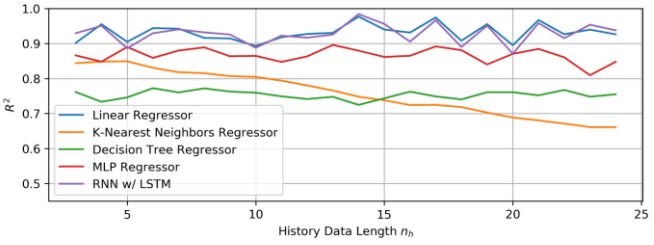

Fig. 5. R^2 scores (higher the better) for the selected regression models with varying history data length n_h.

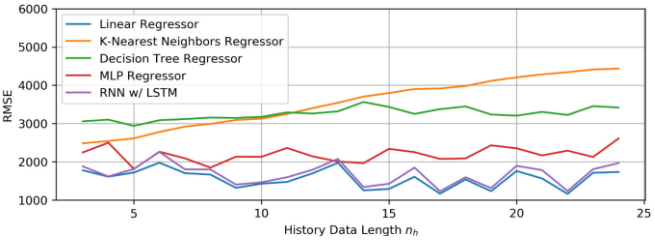

Fig. 6. RMSE (lower the better) for the selected regression models with varying history data length n_h.

Although the RNN with LSTM model has slightly better performance, the main advantages of the linear regression model is that it is much simpler and requires significantly fewer resources [40]. Hence, the linear regression model has been chosen as the best option for the hardware accelerator, which is detailed in Section 6.

It is worth mentioning that the current prediction for one-hour in advance is a case study, which is consistent with the recommended fault detection period of the target SRAM-based SEU monitor [27] and the resolution of historical space flux data from public databases (as shown in Fig. 2, the hourly average flux data are used for energy spectra reconstruction). Estimation and verification of the prediction for several hours in advance will be addressed in our future work, and for that purpose additional in-flight data could be required.

Moreover, due to the fact that an SPE phenomenon is an explosive event, the change of space radiation intensity is abrupt. Therefore, the first SEU instance after the event explosive cannot be accurately predicted only from the detected background SEU data. According to our analysis of all the SPEs in solar cycle 24, the target SRAM SEU rates for the first detected instance after solar event explosive is usually 1.5~6 times higher than the background condition, which is usually less than the recommended self-adaptive

This article has been accepted for publication in a future issue of this journal, but has not been fully edited. Content may change prior to final publication. Citation information: DOI 10.1109/TETC.2022.3147376, IEEE Transactions on Emerging Topics in Computing

mode trigger thresholds, which we introduce in Section 8. In addition, the dependable system would not operate without any protection even at low radiation levels. After detecting the first instance after the event explosive, the proposed one-hour in advance prediction allows to continuously and accurately estimate the forthcoming SEUs. Therefore, the proposed prediction method is suitable for timely adapting the system to the changing environment before the onset of high radiation levels.

5.4 Online Parameter Adjustment

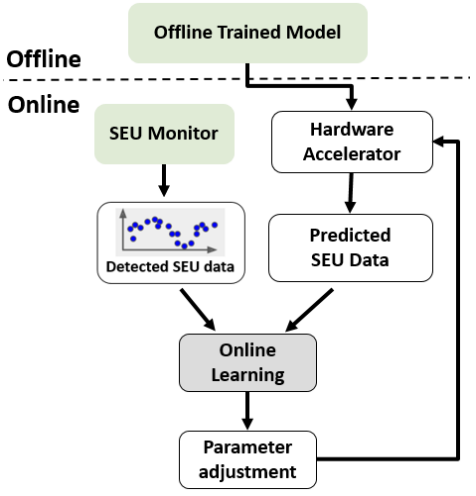

Fig. 7. Block diagram of the proposed online SEU prediction function parameter adjustment procedure.

Since the offline trained machine learning model was obtained according to the historical ion flux data, the proposed model may not perfectly fit the real working environment and could not adapt to a changing environment. For example, in deep-space mission the radiation exposure levels may vary significantly from the SPE levels available in databases used for off-line training. In addition, the SPE databases are available only for a number of possible satellite orbits. Furthermore, the intensity of new SPEs may vary considerably from the data used for training. Therefore, the online learning method is needed to improve the existing offline trained model through learning from the data obtained in the actual working environment. The online learning is good for systems that receive data as a continuous flow and is based on learning autonomously and incrementally from a stream of incoming data. Each learning step is fast and cheap compared to the offline training, thus, the system can learn about the new data on the fly.

In Fig. 7, the online learning process in this study is illustrated. The SEU monitor can perform real-time SEU data detection during the online phase. Therefore, the online system can be trained incrementally by feeding the detected SEU data from the monitor and predicted SEU data from the prediction model sequentially. Thus, the parameters of the offline trained prediction model can be continuously optimized in real-time, thereby, adapt to the changing operating environment.

In this study, the widely used online learning algorithm, Stochastic Gradient Descent (SGD), is used to update the parameters of the selected linear regression model. The SGD performs the gradient descend on a single instance, which is the predicted SEU and the corresponding detected SEU data pair, for each training step. Since very little data is to be manipulated, the SGD algorithm makes the training process very fast. Moreover, only one training instance data needs to be stored in memory at each iteration, which is one of the main reason for the selection of SGD algorithm. For a more detailed SGD description sees [41] for example.

In order to evaluate the SGD online learning performance, the data set used in the offline training was re-used here. The data set was randomly split, where 50% was used to get the initial linear regression offline training model, 30% of the data was used for online learning training and the remaining 20% of the data was used for online learning performance validation. The parameters in the initial linear regression model are the cornerstone of further optimization. The SGD algorithm optimizes the initial model based on the online learning training data set, 1668 instance in this study. The algorithm detail and implementation of SGD in this study are described in detail in Section 6.2. After the SGD performs computing on a single instance each time, the new parameters would be generated and updated to the linear regression SEU prediction model. After learning of each instance, the evaluation is performed in the same approach as described in Section 5.3.

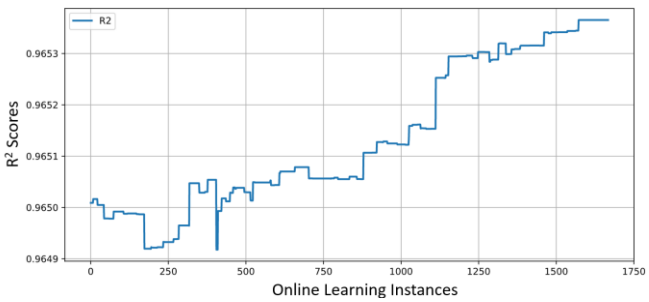

Fig. 8. R^2 score for the online learning evaluation on the data set.

Since only one instance at each online learning step is used, the SGD algorithm is much less regular than the other gradient descent approaches. The cost function of the SGD always bounces up and down and decreasing only on average. Fig. 8 presents the performance in terms of the R^2 score for the SGD training instances on the test data set. It can be noticed that as more instances are processed, despite the evaluation results scores are bounce up and down, the overall prediction performance has been improved. On the other hand, the other important parameter for SGD online learning is the learning rate, which decides the step size at each training step when calculating the descent. If we set the learning rate too small, the optimization process would be slow, while if we choose it too big, the optimization process will be oscillating or cannot even perform the optimization. In this example, a small learning rate is selected, which makes the small variation of scores

This article has been accepted for publication in a future issue of this journal, but has not been fully edited. Content may change prior to final publication. Citation information: DOI 10.1109/TETC.2022.3147376, IEEE Transactions on Emerging Topics in Computing

for each instance. The detail of selecting the suitable learning rate in this study is described in Section 7.2.

The above evaluation shows that the online learning algorithm can gradually improve the prediction accuracy when the online working environment is consistent with the offline analysis environment. In Section 7.2, the online learning application of the other two scenarios are analyzed: when offline flux data are not available, applying online learning directly forms a prediction function from scratch; when the online working environment is not the same as the offline analysis hypothesis, using the online learning to improve the prediction equation.

6 Hardware Accelerator Implementation

The hardware accelerator implements the machine learning algorithm based on the linear regression model and the online learning algorithm based on the SGD. The proposed design is intended to collaborate with an SRAM-based SEU monitor, and the offline-trained results from the linear regression model. Fig. 9 presents the architecture of the proposed hardware accelerator design as well as the connection with collaboration models. Two register files record the detection of real-time hourly SEU data from the monitor and the linear regression training parameters for the SEU data prediction. An accumulator is used to implement the required calculation. The control logic selects the inputs and the functionality of the accumulator as well as the updating of the parameter register file. The right shifter processes the pro-extended data, such as the pre-calculated SEU data from the accumulator to obtain the actual predicted SEU data.

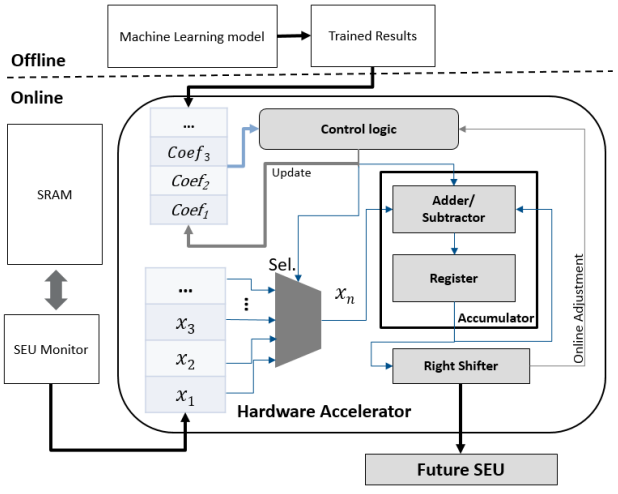

Fig. 9. Proposed hardware accelerator design with interface to external logic.

The calculation flowchart of the hardware accelerator is presented in Fig. 10. It contains two main stages: SEU prediction and the online model parameter adjustment. The two stages are used to implement the selected linear regression module and the SGD algorithm and are explained in following subsections, respectively.

6.1 Single Event Upset Prediction

Based on the results from Section 5.3, the best accuracy of the

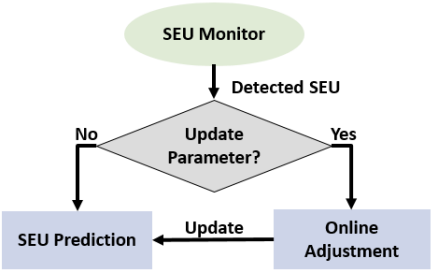

Fig. 10. Decision flowchart for the hardware accelerator.

SEU prediction can be obtained when the history data length of 17 is used. Therefore, the corresponding prediction function for the target SRAM, in this case, can be expressed as:

$$SEU_{pred\_acc} = 1.2929 * x_1 + 0.0868 * x_2 + (-1.1946) * x_3 + 1.0308 * x_4 + 0.1016 * x_5 + (-0.9142) * x_6 + 0.8201 * x_7 + (-0.0178) * x_8 + (-0.6824) * x_9 + 0.6575 * x_{10} + (-0.0204) * x_{11} + (-0.4687) * x_{12} + 0.4181 * x_{13} + (-0.0271) * x_{14} + (-0.2207) * x_{15} + 0.1815 * x_{16} + (-0.0732) * x_{17} \quad (4)$$

The coefficients of Eq. (4) are obtained from the trained linear regression machine learning model. The x_n in Eq. (4) stands for the detected hourly SEU number from the monitor in n hours ago. Thus, the above prediction function can start to predict after the monitor consecutively works and records the first 17 hours of data. Since this design is intended to be used as an embedded part of the spaceborne system, simplicity and flexibility are among the most important concerns. Thus, to avoid floating-point calculation and reduce the hardware complexity, the coefficients in Eq. (4) are magnified by 2^n times and only taking the integer part to simplify the equation. The magnification factor needs to ensure that the new prediction equation induced accuracy variation is less than 1%. In this study, the magnification factor 32 is used, and the corresponding prediction function is as follow:

$$SEU_{pred\_acc\_32} = (41 * x_1 + 3 * x_2 + (-38) * x_3 + 33 * x_4 + 3 * x_5 + (-29) * x_6 + 26 * x_7 + (-1) * x_8 + (-22) * x_9 + 21 * x_{10} + (-1) * x_{11} + (-15) * x_{12} + 13 * x_{13} + (-1) * x_{14} + (-7) * x_{15} + 6 * x_{16} + (-2) * x_{17}) / 2^5 \quad (5)$$

Two 32*21-bit address register files are used for logging the historical SEU data and prediction function coefficients, respectively. Regarding the historical SEU data register file, a single 21-bit entry consists of a valid entry bit, and a 20-bit representing the number of detected upsets. According to the historical solar events analysis for the solar cycle 24, which is introduced in Section 4, the peak value for the hourly upsets count of the target SRAM is 118122 upsets/hour/2Gbit. Therefore, the size of the selected register file can guarantee regular data storage even during large SPE peak fluxes. Moreover, up to 32 historical hourly upsets records can be thus stored simultaneously. If the register file overflows, the oldest individual record will be automatically discarded. For the coefficients register file, the contents are loaded during the system setup and updated after the online parameter adjustment procedure,

This article has been accepted for publication in a future issue of this journal, but has not been fully edited. Content may change prior to final publication. Citation information: DOI 10.1109/TETC.2022.3147376, IEEE Transactions on Emerging Topics in Computing

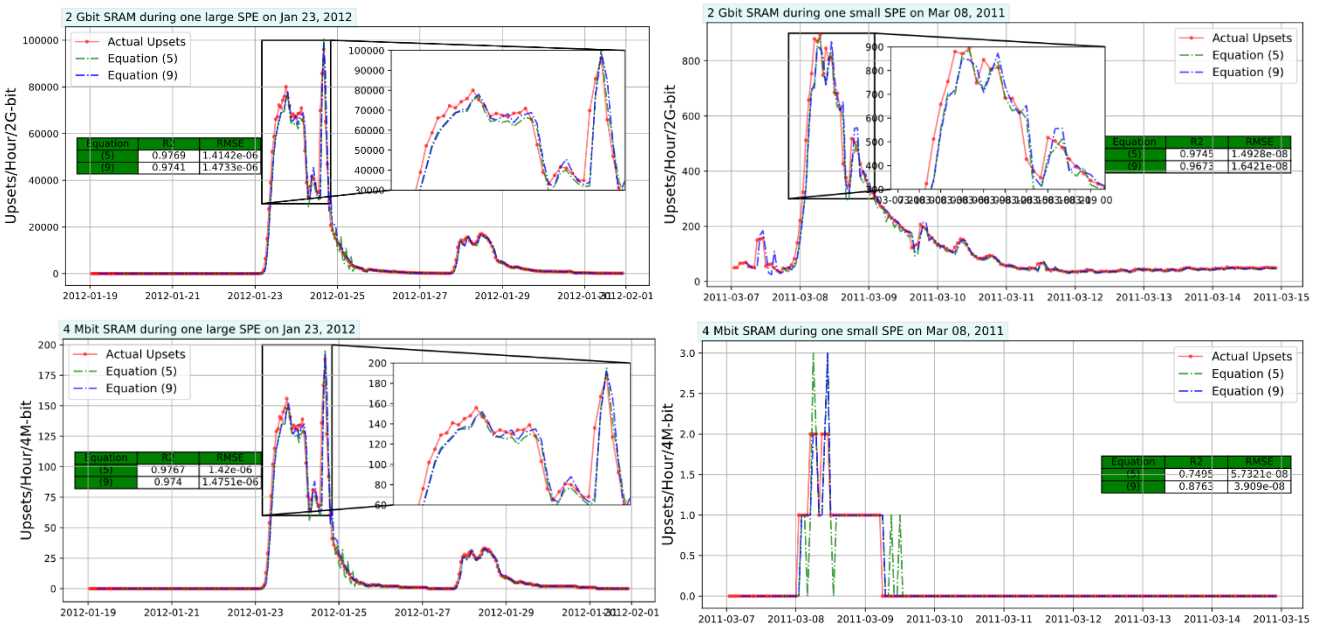

Fig. 11. Hardware accelerator SEU prediction performance for 2Gbit and 4 Mbit SRAM during large and small SPEs, respectively. The equation (5) is the prediction function with history data length 17 and magnification factor 32. The equation (9) represents the prediction with history data length 4 and magnification factor 1024.

which is described in Section 6.2. After being magnified, as shown in Eq. (5), the coefficients are stored in each row, separately.

The accumulator performs repeated addition calculations, thus implementing the multiplication operation in prediction function. Therefore, a much longer calculation time that the traditional multiplier is expected. In this study, for Eq. (5), a total of 262 clock cycles is needed in the accumulator. Therefore, the minimum required time for the calculation of Eq. (5) is 5.24 μs when the working frequency is 50 MHz. As the historical SEU data register file is updated on the hourly basis (i.e. the calculation is required only once every hour), the calculation speed for the accumulator is sufficient for the analyzed application. The accumulator contains a 32-bit full adder, one two´s complement number converter and a 32-bit register. The register keeps the intermediate arithmetic result from the adder. The inputs for adder are the selected x_n and previous results from the register. Moreover, the selected x_n is converted to the two´s complement form when the corresponding coefficient identifies a subtraction operation. Considering the calculation in practical applications, the overflow is not expected.

The control logic processes the coefficients in order to select the appropriate x_n for accumulator, and to determine the number of repetitions in SEU prediction mode. The right shifter is used to shrink the calculation result based on the previous magnified factor, which is 5-bit right shift for Eq. (5).

6.2 Online Parameter Adjustment

The SGD algorithm is implemented here to update the SEU prediction model parameters, thus, adapt to the changing working environment. Due to the simplicity and low-cost purpose of the design, the implementation of the SGD algorithm reuses the sa me hardware design as the SEU prediction work, but with new control logic in the current operation mode. When activated, after a new detected hourly SEU data is received, the online parameter adjustment is performed automatically.

According to the SGD algorithm, the update of each parameter $Coef_j$ in the prediction function is based on the following equation:

$$Coef_j := Coef_j - \alpha \frac{\partial \mathcal{J}(\theta)}{\partial Coef_j} \tag{6}$$

where the α is the learning rate and the $\frac{\partial \mathcal{J}(\theta)}{\partial Coef_j}$ is the gradient of the cost function with regrad to the model parameter $Coef_j$. For the SEU prediction Eq. (5), the corresponding learning rate is set to 0.02, thus, in order to avoid dealing with the floating-point data, the magnified by 2^n times for the learning rate is required. In this study, the magnification factor 256 for the learning rate is selected. Regarding the partial derivative function $\frac{\partial \mathcal{J}(\theta)}{\partial Coef_j}$:

$$\frac{\partial \mathcal{J}(\theta)}{\partial Coef_j} = \frac{\partial (h(x)-y)^2}{\partial Coef_j} = 2(h(x)-y)x_j \tag{7}$$

where the $h(x)$ denotes the predicted SEU data from the selected prediction function, y is the detected corresponding SEU data and x_j stands for the detected hourly SEU data from the monitor in j hours ago. Due to the limitation of hardware resources, the online updating of one prediction function parameter $Coef_j$ is broken down into the following steps:

1) Calculate the error between predicted and observed SEU values E, $E = h(x) - y$;
2) Obtain the corresponding gradient of cost function G_j, $G_j = 2 * \mathrm{E} * x_j$;
3) Multiply by the learning rate, $L_j = \alpha * G_j$;
4) Update the $Coef_j$, $Coef_j := Coef_j - L_j$.

In order to update all parameters, i.e. for Eq. (5), the above

This article has been accepted for publication in a future issue of this journal, but has not been fully edited. Content may change prior to final publication. Citation information: DOI 10.1109/TETC.2022.3147376, IEEE Transactions on Emerging Topics in Computing

steps need to be repeated 17 times. All required calculations are performed by the repeated addition/subtraction in the accumulator and shift register. The overall calculation time greatly depends on the size of x_j in step 2). However, even if all x_j reaches the maximum number, 118122 upsets/hour/2Gbit, the required clock cycle to perform all the calculations is less than 3 M cycles, which corresponds to 0.06 s when the working frequency is 50 MHz. Although the online parameter adjustment requires much longer time than the forecast of SEU, it is still appropriate for this study since the calculation is only needed to perform once an hour.

7 Analysis of Results

7.1 Prediction Performance Analysis

In this section, the impact of SRAM size and history data size for the SEU prediction performance are analyzed. The analysis in Section 6 was done for a large size SRAM with a size of 2 Gbit and with the history data length of 17. However, many embedded systems do not have the multi-Gbit SRAM resources, but rather much smaller internal SRAM with the size from several Mbit to tens of Mbit. In such a case, the small detection area of the SRAM may not provide sufficient sensitivity, and it is necessary to evaluate the optimal SRAM size that is required for particle detection. Moreover, the selection of history data length of 17 means the prediction cannot be done for the first 17 hours, which may be too long for some scenarios where faster prediction is required. According to the history data length analysis in Section 6, length 4 also has an excellent R^2 score with a slightly worse RMSE performance. For this case, the prediction equation is:

$$SEU_{pred\_fast} = 1.1939 * x_1 + 0.1105 * x_2 + (-0.7789) * x_3 + 0.4478 * x_4 \quad (8)$$

The magnification factor 1024 is used for the above function, thus, the corresponding function implemented in hardware accelerator is:

$$SEU_{pred\_fast\_1024} = (1223 * x_1 + 113 * x_2 + (-798) * x_3 + 459 * x_4) / 2^{10} \quad (9)$$

In Fig. 11, the hardware accelerator SEU prediction performance based on functions (5) and (9), for 2 Gbit and 4 Mbit SRAMs, during large and small SPEs, is illustrated. The SEU rate for the 4 Mbit SRAM was determined by scaling the SEU rate for 2 Gbit, i.e. the scaling factor is determined as the size ratio of the two SRAMs. This approach is adopted because the SEU rate is roughly proportional to the SRAM produced in the same technology and using the same bit-cell architectures [42]. However, it is important to mention that this is a rough approximation because the cross-section may differ among different SRAMs. In order to facilitate the comparison of the evaluation scores, the RMSE scores in Fig. 11 are scaled with the corresponding SRAM size.

It can be seen that functions (5) and (9) can predict the SEU variation fairly accurately for the small and large SPEs with 2 Gbit SRAM. However, in the case of 4 Mbit SRAM, only the large SPE can be observed. Neither of these equations can provide sufficient accuracy during a small SPE. The main reason is that the SEU monitor with 4 Mbit SRAM does not have sufficient resolution to provide valid SEU data for prediction during the SPE on-set period.

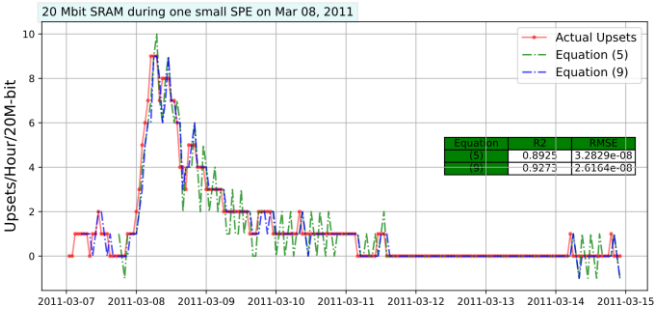

Fig. 12. Hardware accelerator SEU prediction performance for 20 Mbit SRAM during a small SPE on Mar 08, 2011.

In Fig. 12, the prediction performance for 20 Mbit SRAM during the same small SPE as previous is shown. It can be observed that the 20 Mbit SRAM can predict the small SPEs. In addition, due to not considering too much historical SEU data with low resolution, the function (9) has a better prediction performance than function (5). In order to get a smoother prediction curve than in Fig. 12 and thus ensure good quality of SPE prediction, a larger SRAM area needs to be used. In addition, in order to ensure the sensitivity to small variations of space flux, thus, solar condition changes can be accurately detected. We recommend that the SRAM size can guarantee to detect at least one SEU per hour under the background condition. For the target SRAM, the size of 35 Mbit is recommended for online real-time detection.

7.2 Online Learning Performance Analysis

For the online learning process, the learning rate is a critical parameter for the SGD algorithm which determines how fast the system adapts to the changing data. The high learning rate allows the system to quickly adapt to new inputs. However, an excessively high learning rate may induce the system to quickly forget the old data, which may reduce the accuracy. Conversely, a low learning rate makes the system less sensitive to changes in new data. Thus, it is necessary to evaluate an appropriate learning rate for the online parameter adjustment. Moreover, applying online learning to obtain the SEU prediction function from scratch is also analyzed, which is important when the offline training data is not available, such as in deep-space missions. In addition, since the online environment may be inconsistent with the offline analysis hypothesis, the prediction optimization from online learning has also been analyzed.

Fig. 13 presents the gradient descent with the contour plot of the online learning cost function with respect to the SEU prediction coefficients Coef1 and Coef3, which are the two most weighted coefficients in the prediction function,

This article has been accepted for publication in a future issue of this journal, but has not been fully edited. Content may change prior to final publication. Citation information: DOI 10.1109/TETC.2022.3147376, IEEE Transactions on Emerging Topics in Computing

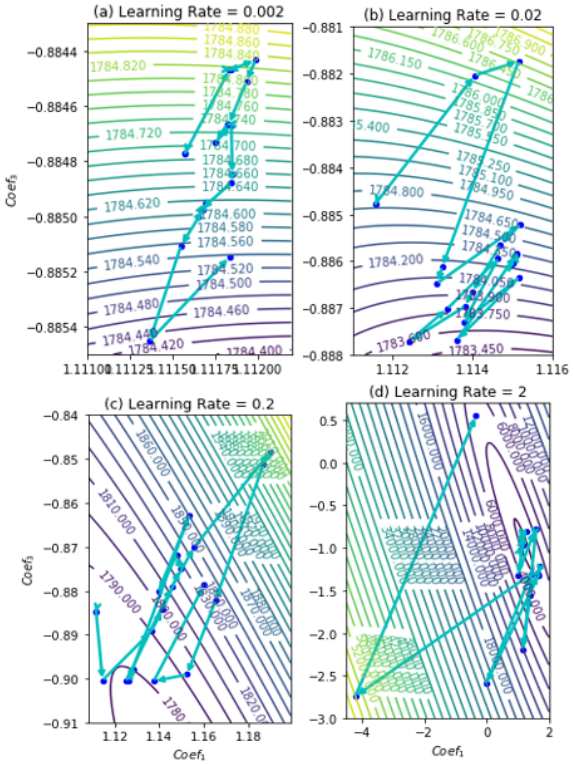

Fig. 13. The gradient descent with contour plot respect to the Coef1 and Coef3 under the different learning rate.

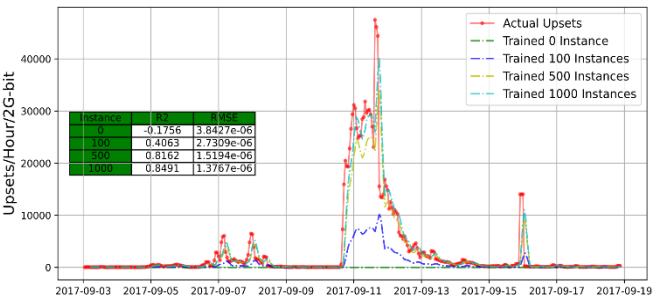

Fig. 14. The prediction performance for online learning from scratch.

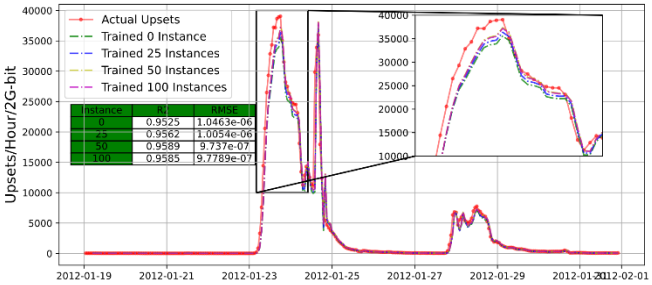

Fig. 15. The prediction performance for online learning optimizes the offline prediction function on the new data set.

regarding the different learning rates. The RMSE cost function was used to perform the analysis. The numbers on the contour line stand for the expected RMSE prediction error with the corresponding coefficients, thus, the smaller the better for the model performance. Four online adjustments with different learning rates were performed, and all of them have the same starting point, where Coef1 is 1.11154 and Coef3 is -0.88478.

It can be found that as the online adjustment progresses, although there will be fluctuations, the prediction errors in Fig. 13 (a) and (b) are steadily decreasing. However, as the learning rate increases in Fig. 13 (c) and (d), the online adjustment could cause a large prediction error, which induces the cliff drop in the prediction performance. The main reason is that a large learning rate may cause abnormal data to have an excessive impact on prediction performance. In addition, the online learning is based on the results from offline training, thus, a small learning rate is more suitable in this study. However, a too-small learning rate could cause a much longer time to adapt to the new working environment. Thereby, the learning rate of 0.02 is selected in this study.

Since the SGD algorithm supports the learning from the new data on the fly, the training approach to abandon offline learning and directly applying online learning to form a prediction function from scratch is possible. In Fig. 14, the prediction performance with the online learning on several amounts of instances for 2 Gbit SRAM is illustrated. The training starts from a linear regression model in which all the coefficients are set to 0. With constant inputs of detected SEU data, the SGD algorithm is used to update coefficients. In this example, it shows that after the SGD algorithm takes about 1000 instances, a relatively well-performing SEU prediction equation can be obtained. Due to the requirement of quickly adapting to a new environment, a high learning rate is expected in the initial stage. However, as the prediction error continues to decrease, the gradually reduce learning rate should perform. Moreover, since the SPE phenomena don't occur frequently, the purely online learning process from scratch could take a long time to achieve a good prediction accuracy for space applications.

The offline training is based on a limited data set and certain parameter assumptions, with may not be the same as the online condition. Thus, in the actual application, there are many other possible reasons that would affect the accuracy of the offline algorithm, such as the actual shielding parameter, changing of the satellite orbits, variation of solar cycles, etc. For example, during the offline data set collection phase in Section 4.3, 100 mils of aluminum shielding were assumed. However, the actual shielding parameters may not be the same. In order to analyze the shielding impacts, a new data set has been collected as the same approach in Section 4, but with a new aluminum shielding parameter, 10 mm (394 mils), which is used in [32]. The prediction function Eq. (5) and the online learning algorithm are used to evaluate the new data set. Fig. 15 shows the new data validation results, and the trained 0 instance means the prediction performance when only uses Eq. (5) for the new data set evaluation. The results

This article has been accepted for publication in a future issue of this journal, but has not been fully edited. Content may change prior to final publication. Citation information: DOI 10.1109/TETC.2022.3147376, IEEE Transactions on Emerging Topics in Computing

show that the prediction based on Eq. (5) has a decline during the SPE peak period, and with the online learning assistance, the forecast results can be gradually improved. Detailed analysis of the performance of online learning in the various environments will be our future work, such as with different orbits, solar cycles, offline analysis parameters, etc.

7.3 Synthesis Results

As the overall idea is to implement the SRAM monitor and hardware accelerator together with the target system on a single chip, it is necessary to investigate the introduced power and area overhead. The synthesis results presented in this Section have been obtained for the IHP's 130 nm bulk CMOS technology with the supply voltage of 1.2V, and the operating frequency of 50 MHz. Although the synthesis analysis in this section uses different technology than the analyzed SRAM, the results are of significant value for hardware consumption comparison because the proposed design is general and can be implemented in different technologies. The choice of the target technology will define the SRAM's cross-section which is obtained from irradiation experiments.

TABLE IV
AREA (IN mm^2) AND POWER (IN mW) COMPARISON

	Area	Power
20 Mbit SRAM	14	384
SEU Monitor	0.0957	0.211
Hardware Acc.	0.6363	3.629

In Table IV, the total area and power consumption for 20 Mbit SRAM, SEU monitor and proposed hardware accelerator are given. Although the power consumption of the proposed hardware accelerator design are about 18 times larger than that of SEU monitor, compared with 20 Mbit SRAM, the induced area and power consumption are only 4.55% and 0.95%, respectively. Moreover, regarding the hardware accelerator, two 32*21-bit address register files are one of the main contributors to the area consumption, which can be reduced in the real case. Besides that, the power consumption for the proposed design is the pessimistic estimation which supposes it always keeps running. However, the hardware accelerator is only expected to perform once an hour, thus, the actual power consumption would be much lower. Thus, these results indicate that the cost and overhead for the hardware accelerator are negligible compared to the host SRAM.

8 Application of the Proposed Design

The proposed design is for the highly dependable and self-adaptive multiprocessing systems employed in space applications, which aims to achieve the trade-off between reliability, power consumption and performance. Due to the inherent hardware redundancy in the multiprocessing systems, the reconfigurable/dynamic mechanisms are convenient for deployment, such as the core-level N-Module Redundancy (NMR), dynamic voltage frequency scaling, dynamic task scheduling, etc. The proposed design can be used for the prediction of the changes in harsh radiation environments. As a result, the optimal operating modes can be selected according to the radiation condition and the reliability requirements.

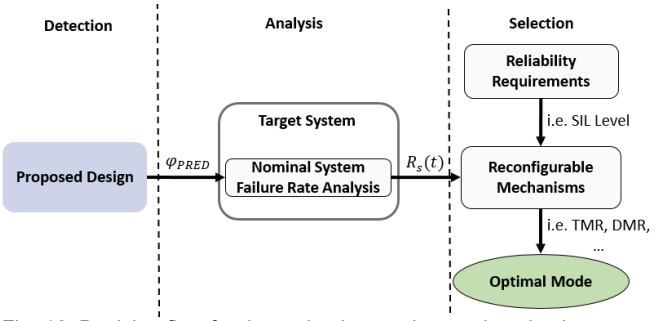

Fig. 16. Decision flow for the optimal operation mode selection.

In Fig. 16, the decision flow for the optimal operating mode selection from the proposed design is illustrated. The proposed decision flow is intended to be used in the self-adaptive platform and contains three main phases: real-time detection, design-phase analysis and real-time mode selection. The goal is to guarantee the reliability of the self-adaptive multiprocessing system. Our proposed design works in the detection phase, which provides the in-flight predicted hourly SEU data.

With the information on the cross-section of SRAM detector, obtained through the irradiation experiment, the predicted particle flux φ_{PRED} in the following time period T (T = 1 hour) can be computed as,

$$\varphi_{PRED} = \frac{SEU_{PRED}}{\sigma_{SRAM} \times T} \tag{10}$$

where SEU_{PRED} is the predicted number of upsets in the target SRAM in the following hour and σ_{SRAM} is the cross-section of the target SRAM and φ_{PRED} is in particle/cm^2.

In the analysis phase, the system failure rate λ_s and reliability function $R_s(t)$ of the target system are computed. The failure rate of the target system depends on the design, operating conditions and particle flux. In terms of operating conditions, the clock frequency and supply voltage affect the failure rate. Higher supply voltage decreases the failure rate due to higher robustness to particle strikes, while higher frequency increases the failure rate due to higher error latching probability. If the system is tested under a predefined nominal flux φ_{NOM}, clock frequency f and supply voltage V_{DD}, the system failure rate under the predicted flux φ_{PRED} can be calculated as,

$$\lambda_{s\_SYS} = \frac{\varphi_{PRED}}{\varphi_{NOM}} \times \lambda_{s\_NOM}(f, V_{DD}) \tag{11}$$

where $\lambda_{s\_NOM}(f, V_{DD})$ denotes the nominal system failure

This article has been accepted for publication in a future issue of this journal, but has not been fully edited. Content may change prior to final publication. Citation information: DOI 10.1109/TETC.2022.3147376, IEEE Transactions on Emerging Topics in Computing

rate for a given frequency and supply voltage. The nominal failure rate can be determined either from irradiation experiments or by simulation/analytical evaluation. If the nominal failure rate is obtained for different operating conditions, a look-up table can be used to store these values and the table readout can be employed to obtain the appropriate value for each operating mode.

For the sake of simplicity, the system failure rate can be denoted as λ_s, i.e. $\lambda_s = \lambda_{s\_SYS}$. Assuming that the system reliability decreases exponentially over time t, the system reliability function $R_s(t)$ can be expressed as:

$$R_s(t) = \mathrm{e}^{-\lambda_s \mathrm{t}} \tag{12}$$

The optimal operation mode should be determined in the selection phase from the system reliability requirements and the available reconfigurable mechanisms during run-time. The IEC 61508 standard [43] proposes four Safety Integrity Levels (SIL), SIL 4 being the most dependable and SIL 1 the least, and is commonly referred by high-reliability systems such as space applications. The Probability of Failures per Hour (PFH) requirements is determined for different SIL levels[1]. The PFH of the system can be calculated by [44]:

$$PFH_s = 1 - R_s(t) \quad \text{with } t = 1h \tag{13}$$

Therefore, from the above equations, the mapping relationship between the SEU_{PRED} and PFH_s can be established, thereby, determining the real-time system SIL based on the radiation condition. As a case study, the proposed design can be integrated into a 4-core multiprocessing system which supports the core-level NMR mitigation technique [5]. Three operating modes are performed in the multiprocessing system:

1) De-stress mode. Three of the cores are powered off and one core is active. Thus, one core system reliability function is:

$$R_{core}(t) = \mathrm{e}^{-\lambda_c \mathrm{t}} \tag{14}$$

2) Fault-tolerance mode. Two, three or all four cores simultaneously execute the same program in a Dual, Triple or Quadruple Modular Redundant (DMR, TMR or QMR) configuration, respectively. According to [45], the corresponding reliability functions are:

$$R_{DMR}(t) = \mathrm{e}^{-2\lambda_c \mathrm{t}} \tag{15}$$
$$R_{TMR}(t) = 3\mathrm{e}^{-2\lambda_c \mathrm{t}} - 2\mathrm{e}^{-3\lambda_c \mathrm{t}} \tag{16}$$
$$R_{QMR}(t) = 4\mathrm{e}^{-3\lambda_c \mathrm{t}} - 3\mathrm{e}^{-4\lambda_c \mathrm{t}} \tag{17}$$

3) High-performance mode. All cores execute different tasks, and the reliability function for each core is equal to Eq. (14).

By adjusting the "redundancy" and "power-off" states of the processing cores to switch operation modes, the system reliability and performance can be dynamically customized. Regarding the radiation-induced transient faults: the DMR enables fault detection at the module output but cannot reduce the system PFH; the TMR can mask one core error and support the decrease of system PFH; the QMR can mask up to two core errors simultaneously, thus, potentially to further attenuation the system PFH.

TABLE V
HOURS PER YEAR SPENT IN DIFFERENT OPERATING MODES ACCORDING TO THE UPSET RATE ($upsets \cdot bit^{-1} \cdot day^{-1}$)

SEU Rate	Operating Mode	Hours / Year
$<10^{-8}$	High-Performance or De-Stress	5460
10^{-8}–10^{-7}	DMR	3120
10^{-7}–10^{-6}	TMR	162
$>10^{-6}$	QMR	18

From the predicted in-flight SRAM SEU, the system PFH can be finally calculated in real-time. Therefore, according to a required SIL level, when the current PFH value exceeds an operation mode-specific threshold during the run-time, the system can load the operation mode autonomously. As an example, table V presents the connection between the predicted SRAM SEU rate and the different operating modes as well as the average hours for corresponding SEU rates in one year average. The SEU rate classification is determined from the published empirical results as seen in Table I, and the accurate SEU rate classification for the mode selection in the target multiprocessing system will be our future work. The average SEU rate duration time in one year is the merging of SEU rates under different solar conditions into a one-year average, detailed in [23].

TABLE VI
POWER COMPARISON OF THE 4-CORE MULTIPROCESSOR UNDER DIFFERENT OPERATION MODES IN ONE YEAR

Operating Mode	Power Consumption
Self-adaptive Mode Switching	12258ρ
De-Stress	8760ρ
DMR	17520ρ
TMR	26280ρ
QMR	35040ρ

In addition to triggering the on-demand operating mode, the proposed self-adaptive mode switching approach can also effectively reduce the power consumption of the target multiprocessing system. Table VI illustrates the power consumption comparison in one year of different operating modes for the target system. The cumulative core energy per year for the self-adaptive mode switching can be calculated as $P_{year} = 5460\rho + 2 * 3120\rho + 3 * 162\rho + 4 * 18\rho = 12258\rho$, where ρ expresses the energy consumption of one core per hour. Comparing with the fault-tolerance modes which have the same performance

[1] *SIL 1: PFH=10^{-5} ~ 10^{-6}; SIL 2: PFH=10^{-6} ~ 10^{-7}; SIL 3: PFH=10^{-7} ~ 10^{-8}; SIL 4: PFH=10^{-8} ~ 10^{-9}*

with the self-adaptive model switching, the power consumption of the proposed approach is even lower than the DMR mode.

9 Conclusion

In this work, an approach for the in-flight SEU prediction of the SRAM-based SEU monitor system in space-borne electronic systems is proposed. Thus, the upcoming flux variation, and the corresponding SPE, can be predicted from the rise of SEU count rate at least one hour in advance. The fine-grained hourly tracking of the SEU variations during the SPE, as well as under normal conditions, is supported. Moreover, the optimization of the prediction function during run-time is realized, thus, the prediction system can adapt to the changing environment. The proposed concept combines the embedded SRAM-based particle detector for online SEU detection, the supervised machine learning prediction model offline trained with the public flux database obtained from past space missions as well as the online optimization algorithm. A dedicated low-cost hardware accelerator for implementing the prediction and online learning system has been proposed, which is intended to support the self-adaptive optimal model selection in the multiprocessing systems. Our analysis has shown that the proposed system has an outstanding prediction accuracy for the analyzed application and with a negligible cost.

A number of open issues have still to be addressed in our future work. Firstly, the prediction accuracy can be further improved, such as providing the real-time measurement of particle LET which can be used as an additional input parameter for the machine learning algorithm. Furthermore, the integration of the proposed prediction system in a self-adaptive multiprocessing system, and verification with irradiation experiments, will be performed.

Acknowledgment

This work has received funding from the European Union's Horizon 2020 research and innovation programme under the Marie Skłodowska-Curie grant agreement No. 72232 as well as the Federal Ministry for Education and Research under the grant 16ME0134.

References

[1] J. L. Barth et al., "Space, Atmospheric and Terrestrial Radiation Environments," IEEE Transactions on Nuclear Technology, Vol. 50, No. 3, pp. 466 – 482, 2003, doi: 10.1109/TNS.2003.813131.

[2] P. E. Dodd, L. W. Massengill, "Basic mechanisms and modeling of single event upsets in digital microelectronics," IEEE Transactions on Nuclear Science, vol., 50, no. 3, 2003, doi: 10.1109/TNS.2003.813129.

[3] R. Harboe-Sørensen, et al., "Observation and analysis of Single Event Effects on-board the SOHO satellite," 2001 6th European Conference on Radiation and Its Effects on Components and Systems, doi: 10.1109/RADECS.2001.1159256.

[4] K. H. Yearby, et al., "Single-event upsets in the cluster and double star digital wave processor instruments," Space Weather, vol. 12, no. 1, Jan. 2014, pp. 24-28, doi: 10.1002/2013SW000985.

[5] A. Simevski, at al, "PISA: power-robust microprocessor design for space applications," in Proc. Int. Sym. on Online Testing and Robust System Design (IOLTS), 2020, doi: 10.1109/IOLTS50870.2020.9159716.

[6] M. Andjelkovic, et al., "A Review of Particle Detectors for Space-Borne Self-Adaptive Fault-Tolerant Systems," 2020 IEEE East-West Design & Test Symposium (EWDTS), 2020, pp. 1-8, doi: 10.1109/EWDTS50664.2020.9225138.

[7] W. S. Wong et al., "Introducing Timepix2, a frame-based pixel detector readout ASIC measuring energy deposition and arrival time," Radiation Measurements, vol. 131, vol. 2, Feb. 2020, Art. No. 106230, doi: 10.1016/j.radmeas.2019.106230.

[8] G. Tsiligiannis, et al., "An SRAM Based Monitor for Mixed-Field Radiation Environments," in IEEE Transactions on Nuclear Science, vol. 61, no. 4, pp. 1663-1670, Aug. 2014, doi: 10.1109/TNS.2014.2299733.

[9] R. Secondo, et al., "Embedded Detection and Correction of SEU Bursts in SRAM Memories Used as Radiation Detectors," in IEEE Transactions on Nuclear Science, vol. 63, no. 4, pp. 2168-2175, Aug. 2016, doi: 10.1109/TNS.2016.2521485.

[10] J. Prinzie, et al, "An SRAM-Based Radiation Monitor With Dynamic Voltage Control in 0.18 um CMOS Technology," IEEE Transactions on Nuclear Science, vol. 66, no. 1, pp. 282-289, Jan. 2019, doi: 10.1109/TNS.2018.2885693.

[11] R. Possamai Basstos, et al., "Assessment of on-chip current sensor for detection of thermal-neutron induced transients," *IEEE Trans. Nucl. Sci.*, vol. 67, no. 7, pp. 1404 – 1411, Jul. 2020, doi: 10.1109/TNS.2020.2975923.

[12] G. Upasani, et al., "A case for acoustic wave detectors for soft-errors," IEEE Trans. on Comput., vol. 65, no. 1, pp. 5 – 11, Jan. 2016, doi: 10.1109/TC.2015.2419652.

[13] M. Bagatin et al., "A heavy-ion detector based on 3-D NAND flash memories," *IEEE Trans. Nucl. Sci.*, vol. 67, no. 1, 154 – 160, Jan. 2020, doi: 10.1109/TNS.2019.2955776.

[14] E. Camporeale, "The challenge of machine learning in space weather: nowcasting and forecasting," Space Weather, 2019, doi: 10.1029/2018SW002061.

[15] H.M. Bain, et al., "Using machine learning techniques to forecast solar energetic particles," Proc. SOARS, 2018, doi: 10.5065/kzsz-vf38.

[16] A.J. Engell, et al., "SPRINTS: a framework for solar-driven event forecasting and research," Space Weather 15 (10) (2017) 1321–1346, doi: 10.1002/2017SW001660.

[17] F. Rocha de Rosa, et al., "Using machine learning techniques to evaluate multicore soft error reliability," IEEE Transactions on Circuits and Systems I: Regular Papers, 2019, doi: 10.1109/TCSI.2019.2906155.

[18] T. Lange, et al, "Machine learning to tackle the challenges of transient and soft errors in complex circuits," Proc. 25th IEEE International Symposium on Online Testing and Robust System Design, 2019, doi: 10.1109/IOLTS.2019.8854423.

[19] S. Hirokawa, et al., "Multiple sensitive volume based soft error rate estimation with machine learning," Proc. European Conference on Radiation and its Effects on Components and Systems (RADECS), 2016, doi: 10.1109/RADECS.2016.8093181.

[20] National Oceanic and Atmospheric Administration (NOAA) solar proton events affecting the earth environment lists, [Online]. Available https://www.ngdc.noaa.gov/stp/satellite/goes/doc/SPE.txt

[21] D. L. Hansen et al., "Correlation of Prediction to On-Orbit SEU Performance for a Commercial 0.25-um CMOS SRAM," in IEEE Transactions on Nuclear Science, vol. 54, no. 6, Dec. 2007, doi: 10.1109/TNS.2007.908787.

[22] Community Coordinated Modeling Center, Coronal mass ejection scoreboard, 2016, http://kauai.ccmc.gsfc.nasa.gov/CMEscoreboard/.

[23] R. Glein et al., "BRAM implementation of a single-event upset sensor for adaptive single-event effect mitigation in reconfigurable FPGAs," 2017 NASA/ESA Conference on Adaptive Hardware and Systems, Pasadena, CA, 2017, pp. 1-8, doi: 10.1109/AHS.2017.8046352.

[24] R. Glein, et al., "Detection of solar particle events inside FPGAs," 2016 16th European Conference on Radiation and its Effects on Components and Systems (RADECS), Bremen, 2016, doi: 10.1109/RADECS.2016.8093159.

[25] J. Chen, et al., "Prediction of Solar Particle Events with SRAM-Based Soft Error Rate Monitor and Supervised Machine Learning," Microelectronics Reliability, Volume 114, 2020, doi: 10.1016/j.microrel.2020.113799.

[26] J. Chen, et al., "Hardware Accelerator Design with Supervised Machine Learning for Solar Particle Event Prediction," 2020 IEEE International Symposium on Defect and Fault Tolerance in VLSI and Nanotechnology Systems (DFT), Frascati, Italy, 2020, doi: 10.1109/DFT50435.2020.9250856.

[27] J. Chen, et al., "Design of SRAM-Based Low-Cost SEU Monitor for Self-Adaptive Multiprocessing System," In Proc. 22nd Euromicro Conference on Digital System Design (DSD), Kalithea, Greece, 2019, doi: 10.1109/DSD.2019.00080.

[28] V. Petrovic, et al., "Design flow for radhard TMR Flip-Flops," Design and Diagnostics of Electronic Circuits and Systems, IEEE International Symposium on, 2015, pp. 203, doi: 10.1109/DDECS.2015.65.

[29] V. Petrović, et al., " Fault-tolerant TMR and DMR circuits with latchup protection switches," Microelectronics Reliability, Volume 54, Issue 8, 2014, Pages 1613-1626, doi: 10.1016/j.microrel.2014.04.001.

[30] Geostationary Operational Environmental Satellites (GOES) - space environment monitor (SEM) database, [Online]. Available https://ngdc.noaa.gov/stp/satellite/ goes/dataaccess.html.

[31] Advance composition explorer (ACE) - solar isotope spectrometer (SIS) database, [Online]. Available http://www.srl.caltech.edu/ACE/ASC/level2/lvl2DATA_SIS. html.

[32] S. E. Hoyos, H. D. R. Evans and E. Daly, "From Satellite ion flux data to SEU rate estimation," in IEEE Transactions on Nuclear Science, vol. 51, no. 5, pp. 2927-2935, Oct. 2004, doi: 10.1109/TNS.2004.835072.

[33] CRÈME96 tool, [Online]. Available https://creme.isde.vanderbilt.edu/.

[34] V. Gupta, "Analysis of Single Event Radiation Effects and Fault Mechanisms in SRAM, FRAM and NAND Flash: Application to the MTCube Nanosatellite Project," PhD dissertation University of Montpellier, 2017.

[35] A. J. Tylka et al., "Single events upsets caused by solar energetic heavy ions," IEEE Trans. Nucl. Sci., vol. 43, pp. 2758–2766, Dec. 1996, doi: 10.1109/23.556863.

[36] J.C. Pickel, et al., "Cosmic-ray-induced errors in MOS devices," IEEE Trans. Nucl. Sci. 27 (2) (1980) 1006–1015. April, doi: 10.1109/TNS.1980.4330967.

[37] F. Pedregosa, et al., "Scikit-learn: machine learning in Python, "J. Mach. Learn. Res. 12 (2011) 2825–2830.

[38] F. Chollet, et al., Keras, [Online]. Available, 2015. https://keras.io.

[39] J. Bergstra, et al., "Random search for hyper-parameter optimization, " J. Mach. Learn. Res. 13 (2012) 281–305 Feb, url: https://www.jmlr.org/papers/v13/bergstra12a.html.

[40] V. Sze, et al., "Efficient Processing of Deep Neural Networks: A Tutorial and Survey," in Proceedings of the IEEE, vol. 105, no. 12, pp. 2295-2329, Dec. 2017, doi: 10.1109/JPROC.2017.2761740.

[41] Q. Cui, et al., "Stochastic Online Learning for Mobile Edge Computing: Learning from Changes," in IEEE Communications Magazine, vol. 57, no. 3, pp. 63-69, March 2019, doi: 10.1109/MCOM.2019.1800644.

[42] Kristian S. et al., "Design and characterization of an SRAM-based neutron detector for particle therapy," Nuclear Instruments and Methods in Physics Research Section A: Accelerators, Spectrometers, Detectors and Associated Equipment, Volume 804, 2015, Pages 64-71, doi: 10.1016/j.nima.2015.09.049.

[43] Functional Safety of electrical / electronic / programmable electronic safety related systems (IEC 61508), International Electrotechnical Com- mission, 2005.

[44] R. Glein, et al., "A Self-Adaptive SEU Mitigation System for FPGAs with an Internal Block RAM Radiation Particle Sensor," 2014 IEEE 22nd Annual International Symposium on Field-Programmable Custom Computing Machines, 2014, doi: 10.1109/FCCM.2014.79.

[45] A. Simevski, et al., "Investigating Core-Level N-Modular Redundancy in Multiprocessors," 2014 IEEE 8th International Symposium on Embedded Multicore/Manycore SoCs, Aizu-Wakamatsu, 2014, doi: 10.1109/MCSoC.2014.33.

Junchao Chen received the M.Sc. degree in electronic engineering from Politecnico di Torino, Italy, in 2017. Since 2018, he has been funded by the Maria Skłodowska-Curie RESCUE ETN project and employed as a member of Prof. Milos Krstic research group in IHP Microelectronics, Frankfurt (Oder), Germany. His research has focused on exploring self-adaptive fault-tolerance mechanisms in multi-core processing architectures, which are backbones of the modern embedded systems. The goal is to enable and explore the dynamic trade-off between reliability, performance and power consumption in the relevant critical applications, such as space applications.

Thomas Lange is an Early Stage Researcher in the RESCUE European Training Network. Within the project he is a Research and Development Engineer at iRoC Technologies, France and a PhD Candidate in Computer and Systems Engineering at Politecnico di Torino, Italy. Thomas holds a Bachelor's and Master's degree in Computer Engineering from Technische Universität Berlin. In his research he is investigating the effects of transient faults for high reliability applications in harsh environments. His main interest includes the development of new models and assessment techniques for transient faults, as well as new mitigation and error management techniques with the focus on hardware capabilities.

Marko Andjelkovic received his Dipl-Ing. degree in Electronics from the Faculty of Electronic Engineering, University of Nis, Serbia, in 2008. Since 2016 he is with IHP, where he is employed as a research associate in the System Architectures Department. His research interests include characterization and modeling of radiation-induced effects in digital circuits, and design of rad-hard solutions. He has participated in several national, bilateral and EU-funded projects, and has authored/co-authored 10 papers in peer-reviewed journals and more than 30 papers at international/national conferences.

Aleksandar Simevski received his Dr-Ing. degree in electronics from Brandenburg University of Technology Cottbus-Senftenberg, Germany (2014). He has been working in IHP since 2010, where he leads several R&D projects in the field of microcontrollers and multiprocessors for space applications. His research and engineering work is focused on dependable processors and multiprocessors with many publications in the field.

Li Lu received the M.Sc. degree in Simulation and Visualization from Norwaigian Univerisity of Science and Techology in 2020. And then she is employed as a member of Prof. Krstic research group in IHP Microelectronics, Frankfurt (Oder), Germany. She worked as an ASIC verification engineer in serveral telecommunication compaies in China from 2009 to 2018. Now her research is focusing on using Machine Learning in improving the dependability of processors.

Milos Krstic received the Dr-Ing. degree in electronics from Brandenburg University of Technology, Cottbus, Germany, in 2006. Since 2001 he has been with IHP Microelectronics, Frankfurt (Oder), Germany, where he leads the System Architectures department. From 2016 he is also professor for "Design and Test Methodology" at the University of Potsdam. For the last few years, his work was mainly focused on fault tolerant architectures and design methodologies for digital systems integration. He has published more than 100 journal and conference papers, and registered seven patents.